Technion - Israel Institute of Technology

Robust Guidance and Control (038781)

Spring 2018

Project 2 - Non-Linear Guidance

Prof. Shaul Gutman

Submitted by : Daniel Engelsman

July 19, 2018

Contents

List of Figures

Introduction

In this project we will explore Non-Linear guidance with Differential Game **(DG)** approach, where a conflict between 2 agents is held and either states evolve according to a set of differential equations. Let us recall the discussed Simulink diagram :

$$G_M(s) = \frac{Ks^2 + KM_\delta}{\tau s^3 + (1+K)s^2 + k_{\dot{v}} M_\delta s + KM_\delta}$$

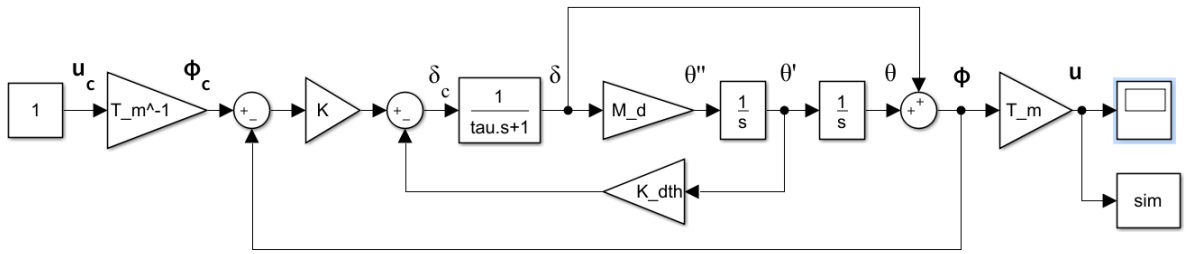

Figure 1: The Auto-Pilot dynamics and its correlated $G_M(s)$

List of Abbreviations

AP	Autopilot
GMD	Guaranteed Miss Distance
MD	Miss Distance
MP	Minimum Phase
NMP	Non Minimum Phase
PN	Proportional Navigation
SR	Step Response
Vc	Closing Speed
ZEM	Zero Effort Miss
ZMD	Zero Miss Distance

1 Guaranteed Miss Distance

1.1 Analytical Solution

Let us consider the following differential game :

$$\begin{aligned} \dot{x} = A(t)x + B(t)u + C(t)v \qquad & Dynamics \\ u \in U, \quad v \in V \qquad & Constraints \\ J = \|Mx(t_f)\| \qquad & Terminal\ Cost \end{aligned} \tag{1.1}$$

Define the Zero Effort Miss variable :

$$\begin{aligned} y = M\Phi(t_f, t)x \qquad & ZEM \\ X(t_f, t) = M\Phi(t_f, t)B(t) \qquad & Pursuer \\ Y(t_f, t) = M\Phi(t_f, t)C(t) \qquad & Evader \end{aligned} \tag{1.2}$$

Using Transition Matrix property we get :

$$\begin{aligned} \dot{y} = X(t_f, t)u + Y(t_f, t)vM \\ since \quad \dot{\Phi}(t_f, t) = -\Phi(t_f, t)A(t) \end{aligned} \tag{1.3}$$

As seen in class, given an optimal strategy pair, each agent will strive to optimize its side :

$$\begin{aligned} \xi' X(t_f, t)p^* = Min\ \xi' X(t_f, t)u \\ \xi' Y(t_f, t)e^* = Max\ \xi' Y(t_f, t)v \\ \alpha(\eta, t) = Min\ \eta' X(t_f, t)u + Max\ \eta' Y(t_f, t)v = \alpha(t) \end{aligned} \tag{1.4}$$

Equivalently, using Euclidean norm we get :

$$p^*(y,t) = -\rho_u(t)\frac{X'(t_f,t)}{\|X(t_f,t)\|}sgn(y) \tag{1.5}$$
$$e^*(y,t) = \rho_v(t)\frac{Y'(t_f,t)}{\|Y(t_f,t)\|}sgn(y)$$
$$\alpha(t) = -\rho_u(t)\,\|X(t_f,t)\| + \rho_v(t)\,\|Y(t_f,t)\|$$

Let us now express each agent's matrix exponent by $\mathcal{L}^{-1}$ transform :

$$G_u(s) := \mathcal{L}(X(t_{go}) = M(sI-A)^{-1}B \tag{1.6}$$
$$G_v(s) := \mathcal{L}(Y(t_{go}) = M(sI-A)^{-1}C$$
$$\alpha(t_{go}) = -\rho_u\left|\mathcal{L}^{-1}\left\{\frac{1}{s^2}G_M(s;F)\right\}\right| + \rho_v t_{go}$$

At last, we can integrate $\alpha(t_{go})$ and obtain optimal path in (y,t_{go}) space :

$$|y| = |y(0)| + \rho_u\int_0^{t_{go}}\mathcal{L}^{-1}\left\{\frac{1}{s^2}G_M(s;F)\right\}d\rho - \frac{1}{2}\rho_v t_{go}^2 \tag{1.7}$$

We'll define t_{go} variant as $\Theta = \{t_{go} \geq 0 : \alpha(t_{go}) = 0\}$ and get :

$$\Theta = \frac{1}{t_{go}}\left|\mathcal{L}^{-1}\left\{\frac{1}{s^2}G_M(s;F)\right\}\right| = \frac{\rho_v}{\rho_u} = \mu \qquad \forall\, ||\mu|| < 1 \tag{1.8}$$

Where μ is the acceleration ratio between evader and missile. In addition we'll define :

$$\hat{m} = Max\left\{-\rho_u\int_0^{t_{go}}\mathcal{L}^{-1}\left[\frac{1}{s^2}G_M(s;F)\right]d\rho - \frac{1}{2}\rho_v t_{go}^2\right\} \tag{1.9}$$

Where $\hat{m}$ is the Guaranteed Miss Distance.

1.2 Simulink Implementation

In this section we will realize the above equations into a Simulink models :

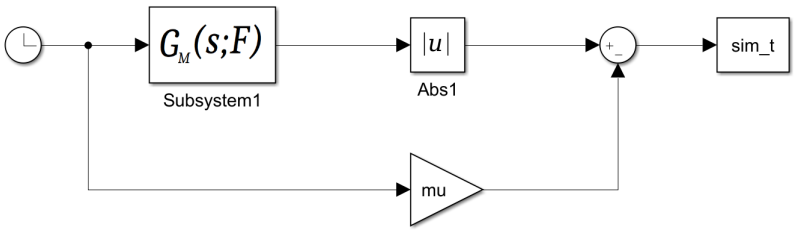

Figure 2: Simulink Model of Eq. (8)

Running the compatible simulation of Θ where $\mu \in [0.1\ 1]$:

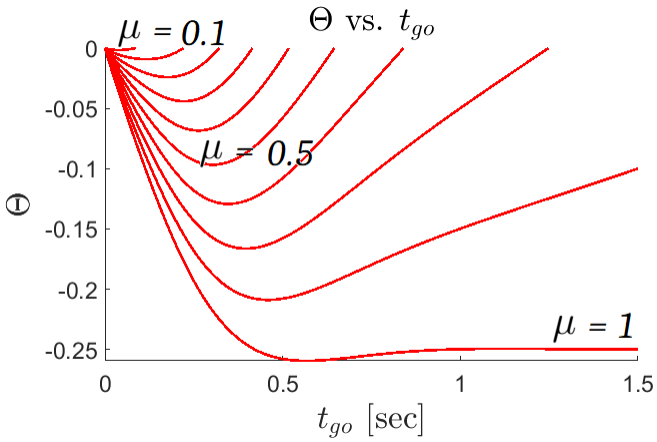

Figure 3: Simulation of Θ vs. t_{go}

Similarly, we will design the $\hat{m}$ adjoint :

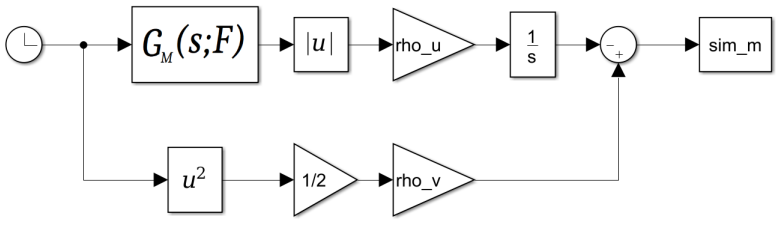

Figure 4: Simulink Model of Eq. (9)

And here, running the compatible simulation of $\hat{m}$ where $\mu \in [0.1\ 1]$:

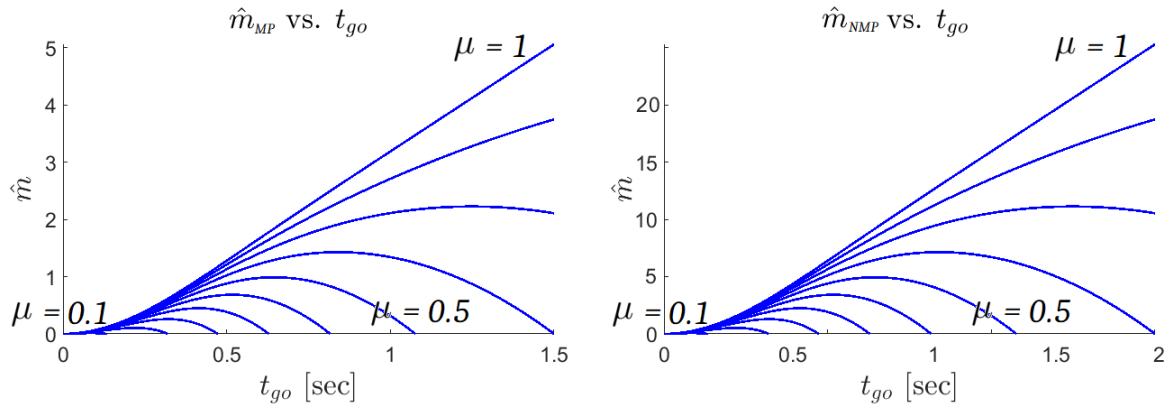

Figure 5: **Left :** MP $\hat{m}$ vs. t_{go} **Right :** MP

Let us concentrate the Guaranteed Miss Distance (GMD) in a table :

μ	t^s_{go} [sec]	m^*_{MP} [m]	t^s_{go} [sec]	m^*_{NMP} [m]
0.1	0.10	0.0139	0.13	0.0785
0.2	0.23	0.1047	0.31	0.3532
0.3	0.33	0.2574	0.45	0.7848
0.4	0.43	0.4482	0.56	1.2753
0.5	0.53	0.6841	0.72	2.0601
0.6	0.66	0.9894	0.91	3.2373
0.7	0.85	1.4289	1.04	5.4936

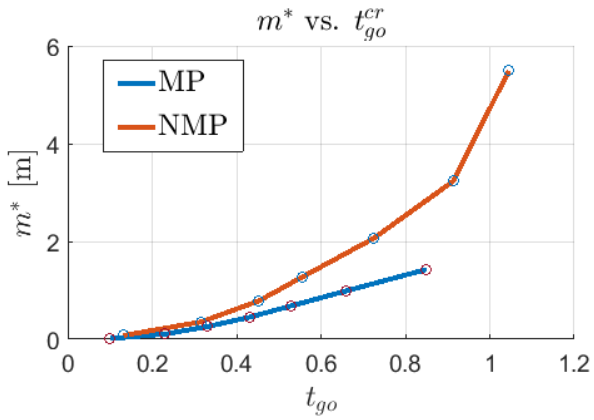

Figure 6: Table of $\hat{m}$ vs. t^s_{go} due to different μ

The above graph (**Fig**. 9) will use us **in turn** to execute the adjoint simulation. Every pick of $\hat{m}$ path is coupled with its compatible (t^s_{go}, μ), and later will be used in the simulation.

1.3 Parametric Analysis

After running few simulation in sought after GMD's sensitivity, I will hereby show influence of some parameters on the guaranteed miss distance. **Important Notes :**

(i) Both configurations showed the same tendency / reaction in absolute values. I will therefore take the MP configuration as the study case, that speaks also for NMP.

(ii) For the sake of convenience I chose $\mu = 0.5$ for the simulations, otherwise when $\mu \simeq 0$ the pursuer agility is too strong, and blurring any other parameter's influence.

(iii) Tests are in comparison with a default value of ($\mu = 0.5$, $t_{cr}^{MP} = 0.53, m_{MP}^{*} = 0.6841$).

First to go is the M_δ parameter when $|y(t_f)|$ is normalized. **Default** : first from left.

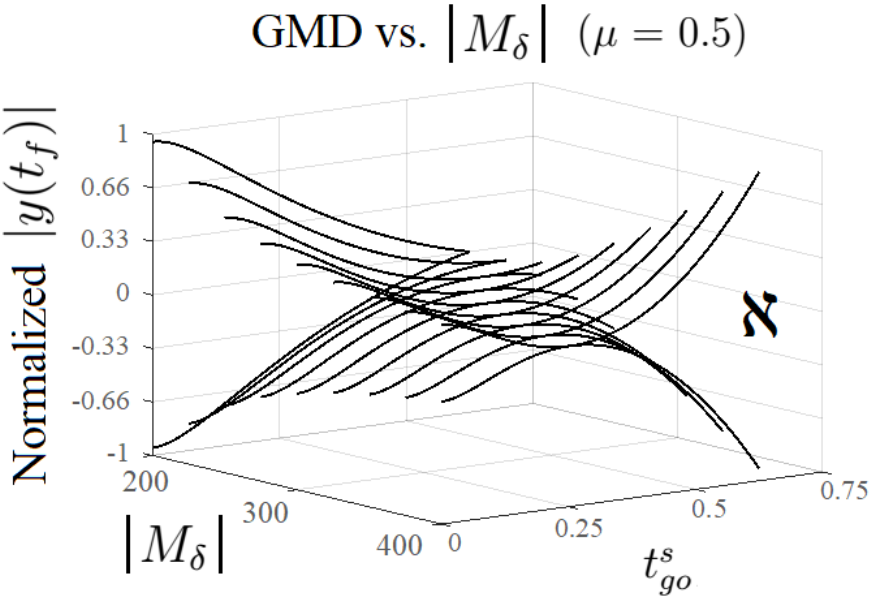

Figure 7: State Space Decomposition $|y(t_f)| = f(M_\delta)$

We see that the arbitrary zone increases as follows ($M_\delta \uparrow$, $|y(t_f)| \downarrow \quad \Rightarrow \aleph \uparrow$) in favour of the pursuer. That allows him staying more time on linear strategy (PN/APN), and oppositely, the target is now coerced to perform the maneuver only a **moment** before capture.

Let us now check the GMD sensitivity to the servo's τ. **Default** : first from right.

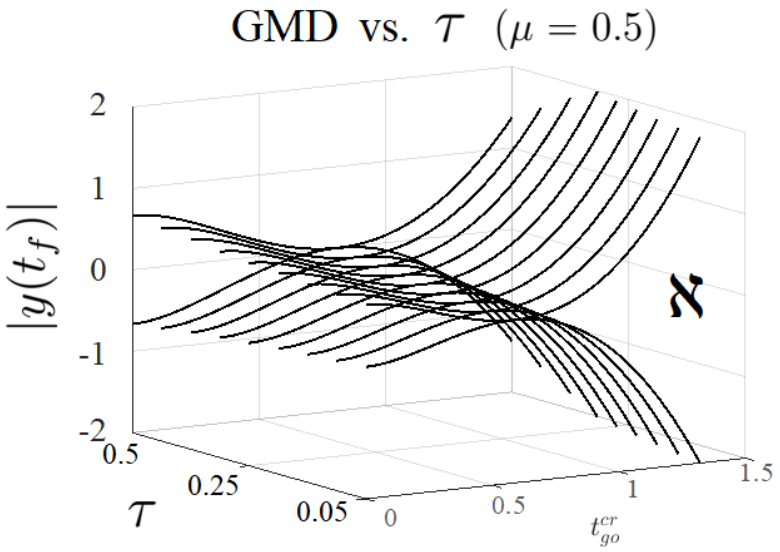

Figure 8: State Space Decomposition $|y(t_f)| = f(\tau)$

As shown, less dramatically than M_δ, but still shows a notable tendency when τ increases. We get that ($\tau \uparrow$, $|y(t_f)| \uparrow \ \Rightarrow \aleph \downarrow$), meaning that longer τ slows the agility of the pursuer and gives the target more time to perform the maneuver (MD $\uparrow$). Next is the $(\frac{T}{m})$:

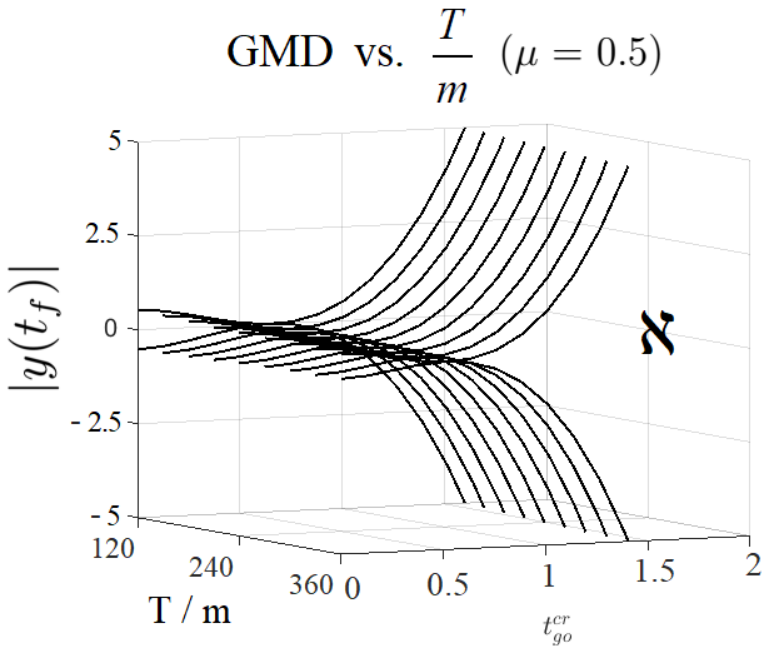

Figure 9: State Space Decomposition $|y(t_f)| = f(\frac{T}{m})$

Default : first from left. This time the GMD is rather indifferent to the longitudinal acceleration. It is indeed improves slightly the obtained results, yet very little in comparison to the pervious parameters.

1.4 Discussion

One can see a correlation between the acceleration ratio "μ" and the obtained response family. Each of these "family members" expresses the optimal trajectory's contact point upon the t_{go} axis, at time t_{go}^s.

At both configurations when accelerations ratio are in the vicinity of $\mu = 1$, we see that $t_{go}^s \to \text{inf}$. That is to say that contact will hardly occur, and the initial condition of distance and velocity will decide the capture.

Oppositely, when μ decreases towards "0" so does $t_{go}^s \to 0$, as it expresses the pursuer supremacy over the evader, and the conquer of ℵ over the space. Therefore, t_{go}^s timing is significantly influenced by μ magnitude.

2 Compute and Calculate $N^* \in [\theta_s, \infty]$

2.1 Analytical Solution

The optimal navigation constant can be constructed via development of the ZEM :

$$y = M\Phi x = \begin{bmatrix} 1 & t_{go} & \mathcal{L}^{-1}\{\widehat{c}(sI - \widehat{A})^{-1}/s^2\} \end{bmatrix} \begin{bmatrix} x_1 \\ x_2 \\ z \end{bmatrix} = t_{go}^2 \left[V_c\dot{\sigma} - \frac{1}{t_{go}^2}\mathcal{L}^{-1}\{(\widehat{c}(sI - \widehat{A})^{-1}/s^2\}z \right] \tag{2.1}$$

The linear strategy in the "Arbitrary zone" of the $(|y|, t_{go})$ plane, has the form $u_c = Ky$:

$$K = \frac{\rho_u}{m + \int_{t_{go}}^{t_{go}^s} |\mathcal{L}^{-1}[G_M(s;F)/s^2]|d\rho - \frac{1}{2}\rho_v[t_{go}^2 - t_{go}^{s\,2}]} \tag{2.2}$$

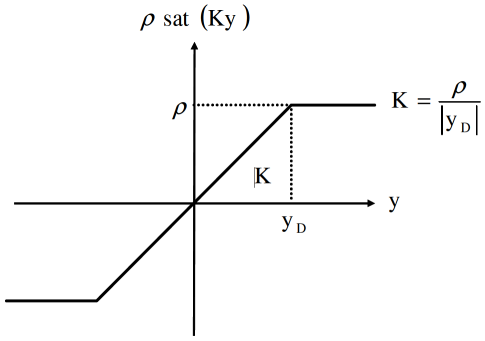

Figure 10: Saturation

Combining (2.1) and (2.2) and we get for $t_{go} > t_{go}^s$:

$$u_c = \rho_u sat\{N^*(V_c\dot{\sigma} - N_a z)\} \tag{2.3}$$

Extracting N^* where $\mu = \frac{\rho_v}{\rho_u}$:

$$N^* = \frac{t_{go}^2\, sgn[\,\mathcal{L}^{-1}\{G_M(s;F)/s^2\}]}{\frac{m}{\rho_u} + \int_0^{t_{go}} |\mathcal{L}^{-1}[G_M(s;F)/s^2]|d\rho - \frac{1}{2}\mu t_{go}^2} \tag{2.4}$$

2.2 Simulink Implementation

And now, in order to execute the mentioned above (**Eq.** 2.4), let us design the compatible implementation on Simulink :

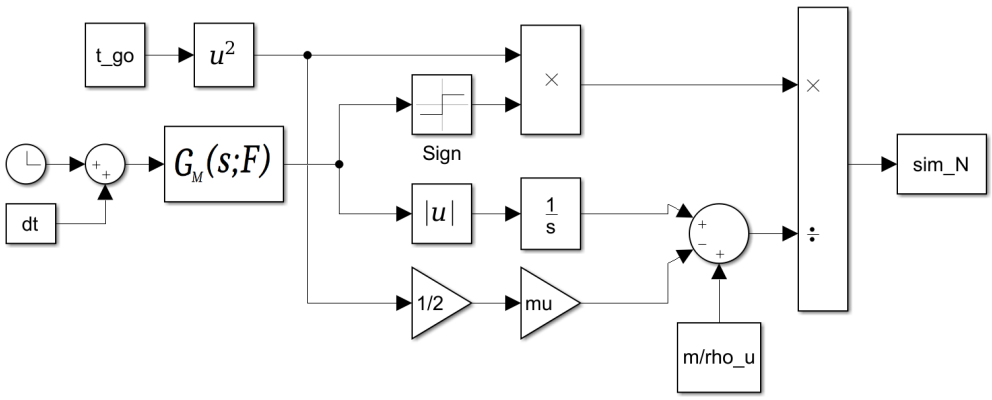

Figure 11: N^* vs. t_{go} @ NMP

Plugging the values from table at **Fig.** 9 into the compatible blocks in a growing sequence $(\mu_1 \dots \mu_n)$, and running each of the configuration (MP, NMP) :

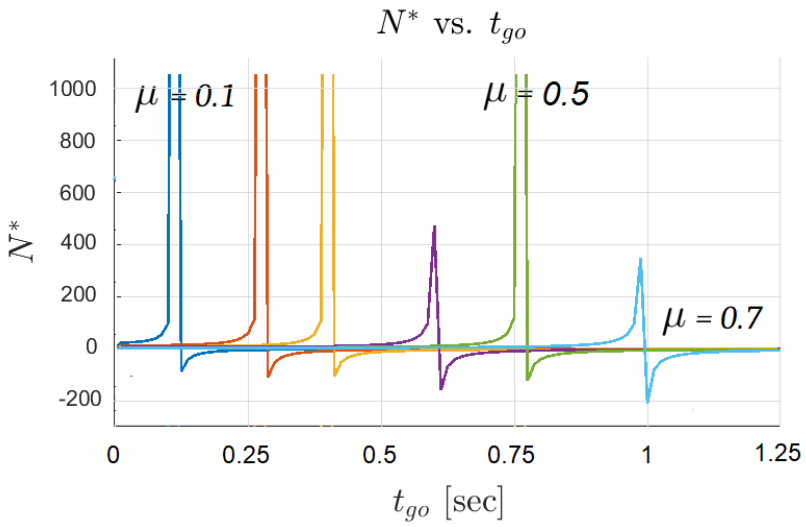

Figure 12: N^* vs. t_{go} @ MP

We can see that N* is rather low prior to $t_{go} > t^s_{go}$ and can be explained by the ℵ domain thet enables linear strategy (PN / APN). At the very $t_{go} = t^s_{go}$, N* rises sharply in response to the target critical maneuver, and afterwards becomes optimal until final capture $t_{go} = 0$.

When running NMP, we get opposite response that exhibits also a divergence of $N^* \rightarrow |\infty|$. As seen on table at **Fig.** 9, there is $t^s_{NMP} > t^s_{MP}$ that is expressed also on t^s_{go} timings.

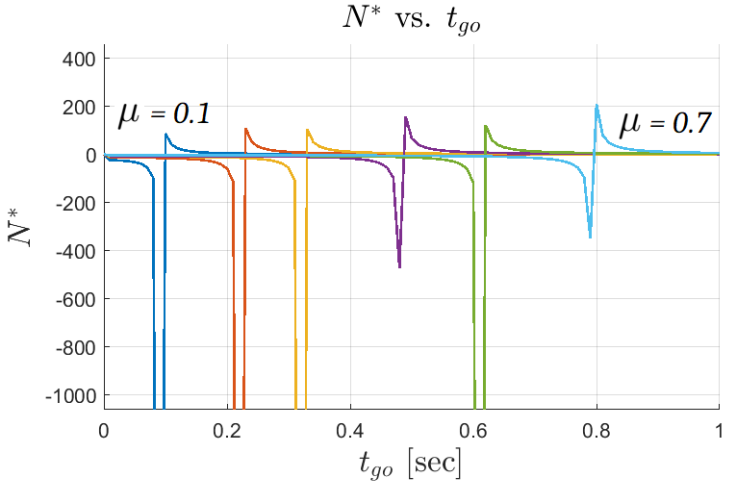

Figure 13: N^* vs. t_{go} N^* vs. t_{go} @ NMP

The leftest plot belongs to $\mu = 0.1$, where the pursuer is most agile, while the rightest fits with $\mu = 0.7$, where the evader accelerates slightly less from the pursuer.

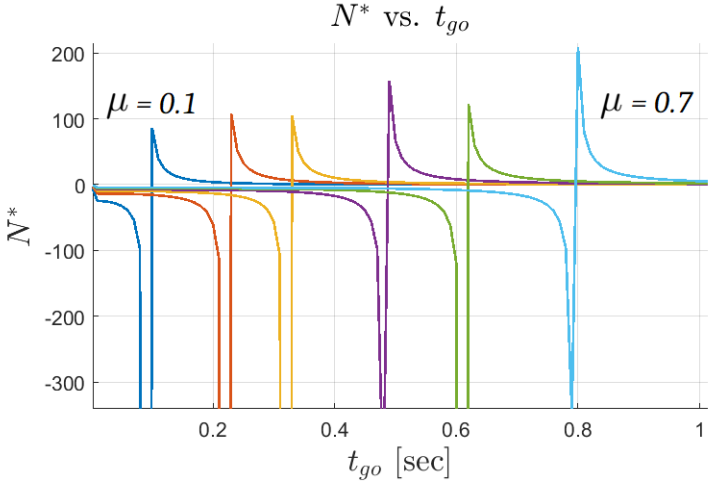

Figure 14: N^* vs. t_{go}

When can see the dramatic N^* "spikes" in the vicinity of each compatible t^s_{go}. **Note** that after these spikes, N^* shows downfall, but it is no longer relevant, and stems from the mathematical solution.

2.3 Analysis of N^*'s Nature

Based on **Eq**. 2.4 we'll examine what happens along t_{go}, and thus lead to the dramatic results. This time we'll take a close look at the limits.

The dynamics' step function after it settles equals to "1". Here with $[\frac{1}{s^2}]$ input :

$$\lim_{t_{go}\to\infty} \mathcal{L}^{-1}[G_M(s;F)/s^2]| = \lim_{t_{go}\to\infty} \mathcal{L}^{-1}[(1)\cdot\frac{1}{s^2}]| = \lim_{t_{go}\to\infty} t_{go}$$
$$Therefore : \int_{t_{go}}^{\infty} \lim_{t_{go}\to\infty} |\mathcal{L}^{-1}[(1)\cdot\frac{1}{s^2}]| = \int_{t_{go}}^{\infty} t_{go} = \frac{1}{2}t_{go}^2 \tag{2.5}$$

$$\lim_{t_{go}\to\infty} N^* = \lim_{t_{go}\to\infty} \frac{t_{go}^2\, sgn[\,\mathcal{L}^{-1}\{G_M(s;F)/s^2\}]}{\frac{m}{\rho_u} + \int_0^{t_{go}} |\mathcal{L}^{-1}[G_M(s;F)/s^2]|d\rho - \frac{1}{2}\mu t_{go}^2} \tag{2.6}$$

Combining Eq. (2.5) :

$$\lim_{t_{go}\to\infty} N^* = \lim_{t_{go}\to\infty} \frac{t_{go}^2(\, sgn[\,\mathcal{L}^{-1}\{G_M(s;F)/s^2\}])}{t_{go}^2(\frac{m}{\rho_u t_{go}^2} + \frac{1}{2} - \frac{1}{2}\mu)} = \frac{(\pm)1}{(\frac{m}{\rho_u t_{go}^2} + \frac{1}{2} - \frac{1}{2}\mu)} \tag{2.7}$$
$$And \quad eventually \quad : \lim_{t_{go}\to\infty} N^* = \frac{(\pm)1}{\frac{1}{2}(1-\mu)} = \frac{(\pm)2}{(1-\mu)}$$

Note : The $(\pm)$ sign denotes the relevant configuration, that here yielded almost the same results. Plugging values and concentrating in table, we get that :

μ	t_{go}	N^*_{MP}	N^*_{NMP}
0.1	∞	2.222	-2.222
0.2	∞	2.500	-2.500
0.3	∞	2.857	-2.857
0.4	∞	3.333	-3.333
0.5	∞	4.000	-4.000
0.6	∞	5.000	-5.000
0.7	∞	6.667	-6.667

We see that N^* approaches values as low as it gets in **PN**. Is this considered as **Optimal** ?

Discussion

Let us recall **Eq.** 1.6 :

$$\alpha(t_{go}) = -\rho_u \left| \mathcal{L}^{-1}\left\{ \frac{1}{s^2} G_M(s;F) \right\} \right| + \rho_v t_{go}$$

When α is integrated, it spans an optimal path (trajectory) in the (y,t_{go}) space (AKA game space). The D_1 / ℵ region, forces any trajectory to pass through (t^s_{go},0) and follow optimal path towards (0,m^*). Hence, expressing shift from *linear* to *optimal* Strategy.

When $t_{go} \geq t^s_{go}$:

$$\lim_{t_{go}\to\infty} N^* \sim N_{PN}$$

Meaning that u^* is arbitrary admissible to be any **linear strategy** in D_1 or ℵ at my figures.

Contrarily, when $t_{go} \leq t^s_{go}$:

$$\lim_{t_{go}\to t^s_{go}} |N^*| = \infty$$

Meaning that outside D_1 we are forced to use **bang-bang** or any other **optimal** policy that is coerced until end of the flight time.

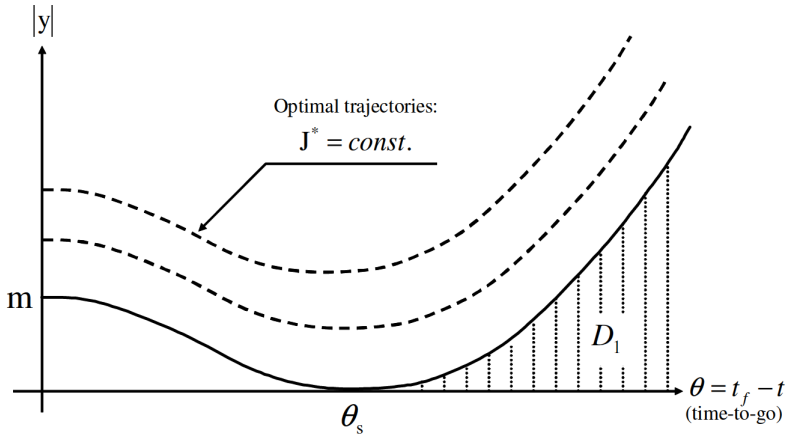

Figure 15: State Decomposition

3 N^* when $m_r \geq m^*$

Given a scenario where $m_r \geq m^*$, let us first portray the $(\|y\|, t_{go})$ plane and its curves family as long as they don't intersect y=0 :

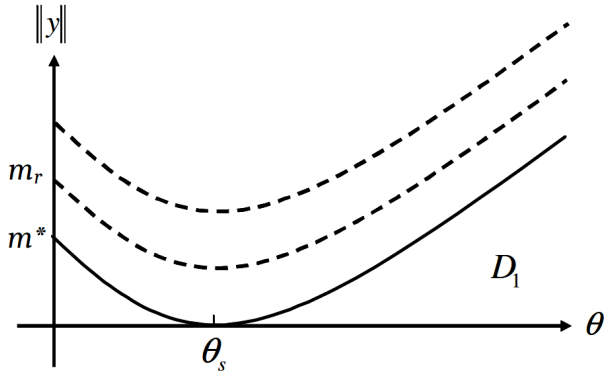

Figure 16: Trajectory of $\|y(t_F = 0)\| = m_r$

In order to simulate it, we'll go back to the Simulink model in Fig. 7, and within every iteration change the following :

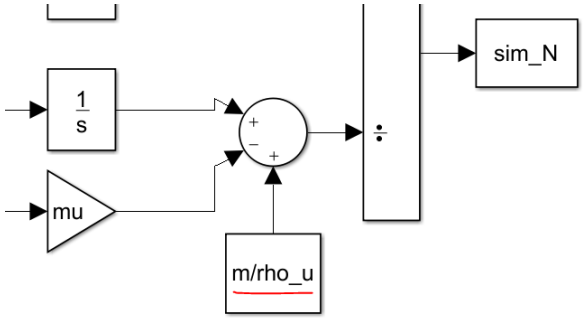

Figure 17: Changing $m*$ within every iteration

The m/ρ_u ratio and the y_0 initial condition at the integrator, in order to apply a growing "constanta" every iteration. Hence, the pursuer **Guidance requirements** are now softer than before.

So now let us run the N^* simulations where m_r is in an increasing sequence :

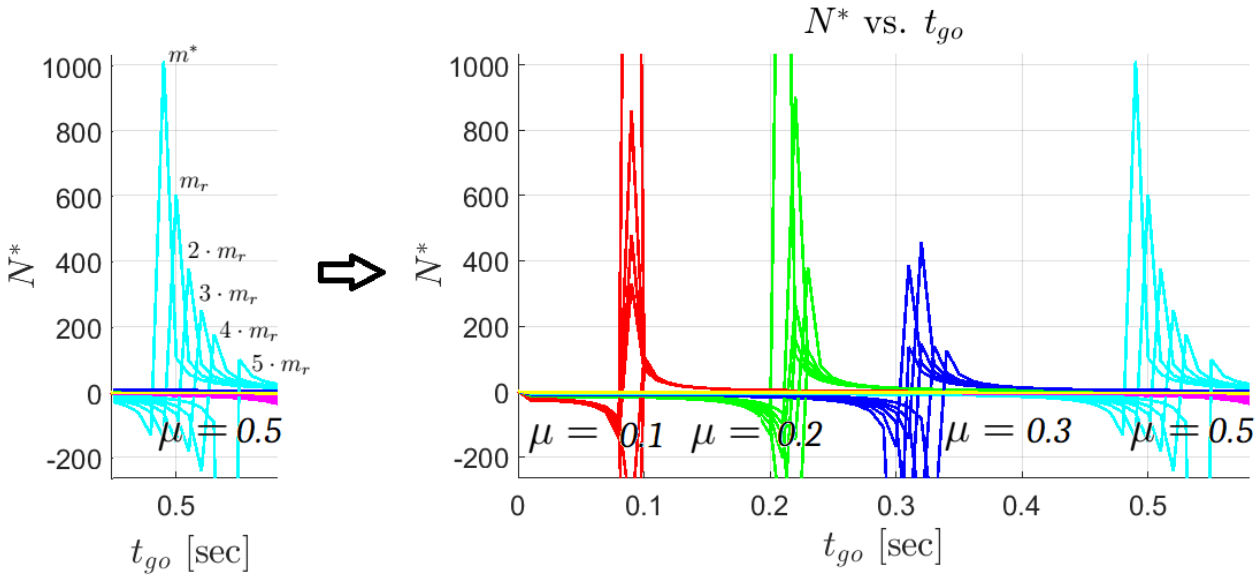

Figure 18: Declination of N^* as function of m_r

As expected, when the required miss distance m_r is bigger than the optimal MD m^*, our system is able to get that result - at **smaller** N^* magnitudes. As seen, the leftest / highest graph of each "bulk" $\mu \in [0.1,...,0.7]$, denotes the **optimal path** that results in m^*. Going right / down, we get N^* declination in magnitude in concordance with m_r inclination.

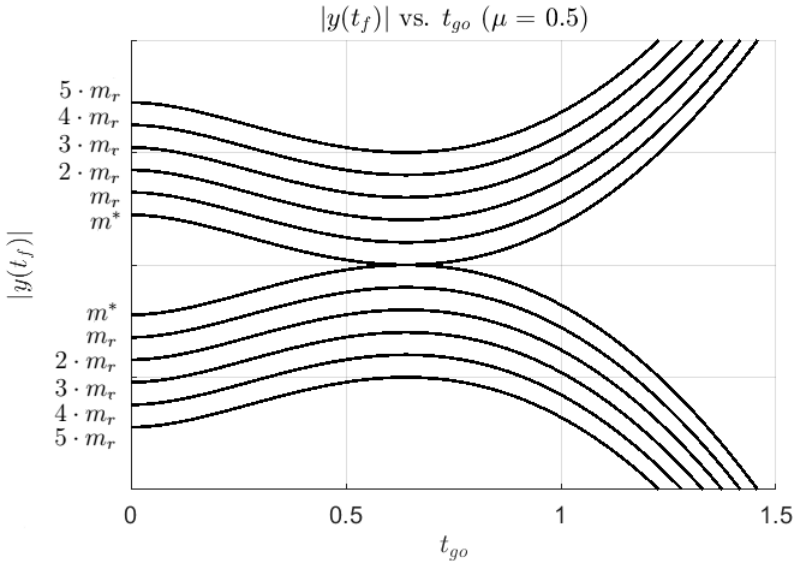

Figure 19: State Decomposition follows ($m_r \uparrow$, $N^* \downarrow$)

4 δ_c Saturation

Aerodynamic wise, every airfoil has a bounded operation range depends on its angle of attack and the reltaive velocity of the flow field. Beyond a certain angle, the flow separates from the airfoil layer and **stall** occurs, meaning that the airfoil becomes useless.

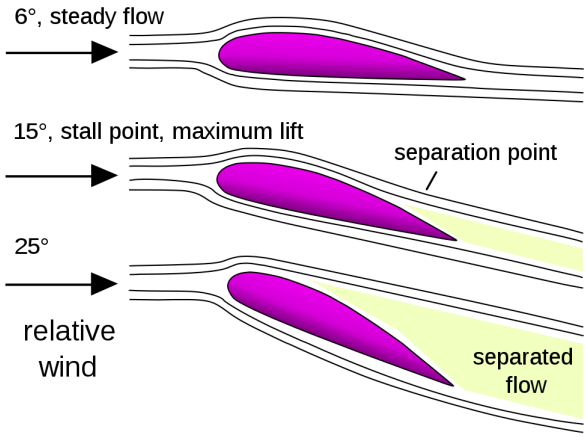

Figure 20: Flow upon Airfoil vs. angle of attack

This phenomenon permeates down to the pursuer's guidance performance, since it imposes hard boundary limits on δ_c. Let us build a PN guidance loop :

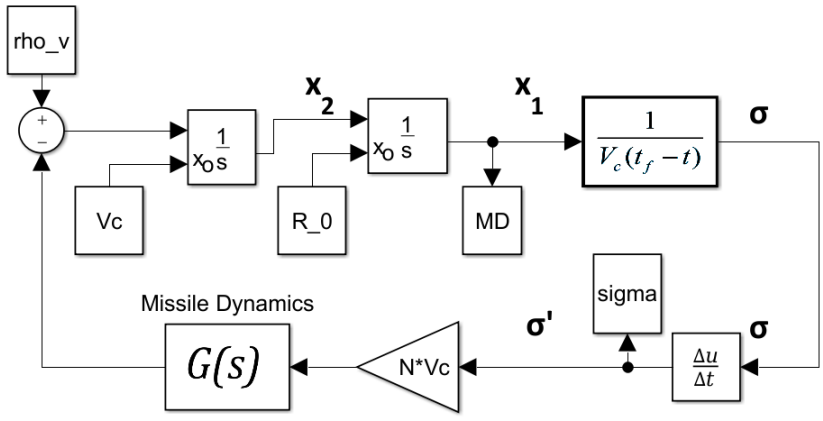

Figure 21: Saturated Proportional Navigation

Let us recall in the LOS angle that defines the orientation of the pursuer towards to evader :

$$\sigma = \frac{x_1}{R} \qquad \rightarrow \qquad \dot{\sigma} = (\frac{\partial}{\partial t})\sigma = \frac{x_1 + t_{go}x_2}{V_c t_{go}^2} \tag{4.1}$$

When pursuer reaches $t \rightarrow t_f$, the following conditions are satisfied at the limit :

$$\lim_{t_{go}\to 0} \dot{\sigma} = \frac{\cancelto{0}{x_1} + t_{go}x_2}{V_c t_{go}^2} = \frac{x_2}{V_c \cancelto{0}{t_{go}}} = \infty \tag{4.2}$$

Meaning that the very last moment before contact, the pursuer is subjected to large $\dot{\sigma}$:

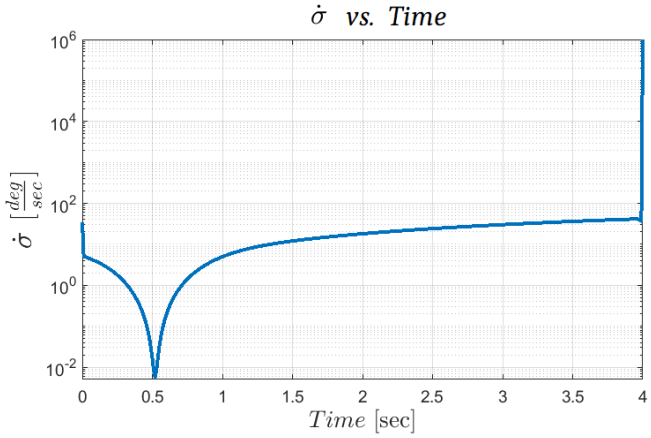

Figure 22: LOS angular rate vs. Time

Along the flight time, the LOS rotates at reasonable rates of several $[\frac{deg}{sec}]$. But when $t_{go} \rightarrow 0$ we have a sudden peak which obviously cannot be fulfilled by the pursuer. That huge $\dot{\sigma}$ is translated into a mechanical command δ_c. Dashed line denotes servo's limit ($\delta \leq 30[\frac{deg}{sec}]$) :

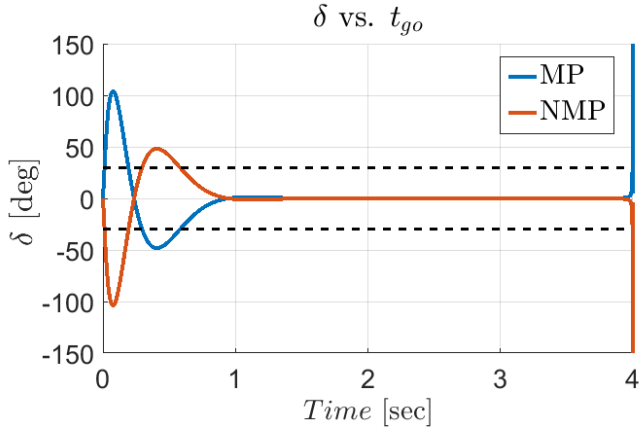

Figure 23: δ vs. Time

The Servo's deflection in the linear simulation crosses the mechanical boundaries of the servo ($|\delta| \leq 30$ [°]), and in the "real" world would **lock** the servo at **Maximum** angle. This phenomenon is **Dangerous** for the mechanical loads on the one hand, and the **stall** effect on the other that turn the airfoil into useless.

Avoidance

In order to avoid that unreasonable rotation angles, one must limit the servo's commands $\delta_c \leq \delta_{MAX}$ to the mechanical limit :

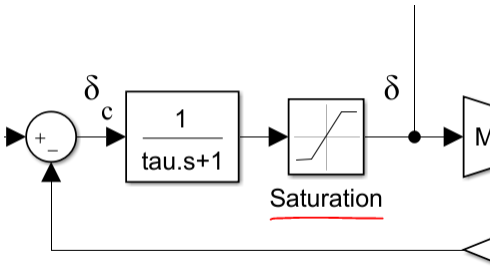

Figure 24: Saturation block at the auto-pilot

This way we can ensure that no **mechanical violations** occur during flight time and the commands stay at the safe zone of the elements :

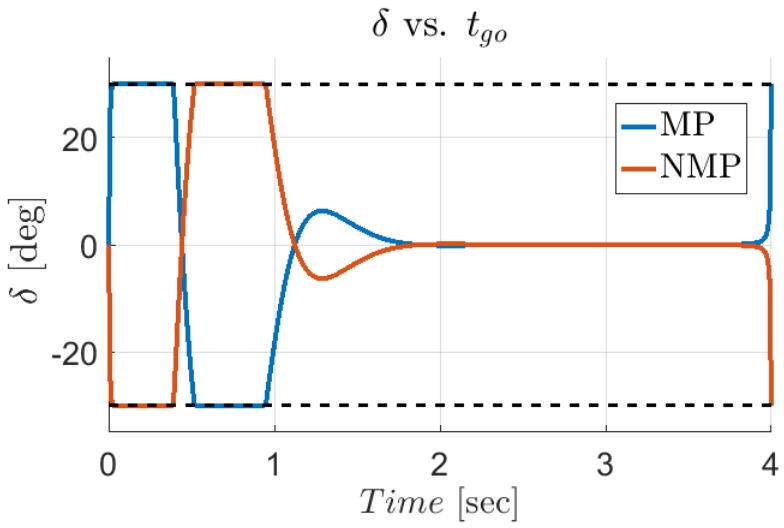

Figure 25: Saturated δ vs. Time

Let us now look at the influence of the servo's saturation upon the miss distance :

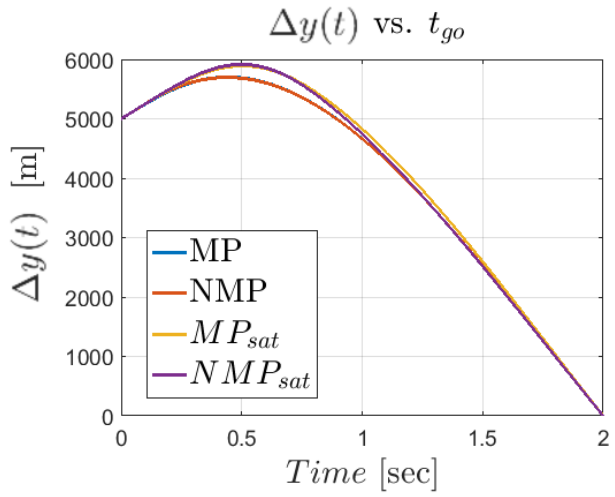

Figure 26: Trajectories of Unsaturated and Saturated δ

We can see that the upper arc (Saturated) shows slightly poorer results since it is more limited and thus pefroms worse maneuver. Looking closer we will see the expected distribution between MP / NMP performances, just as we've so far seen :

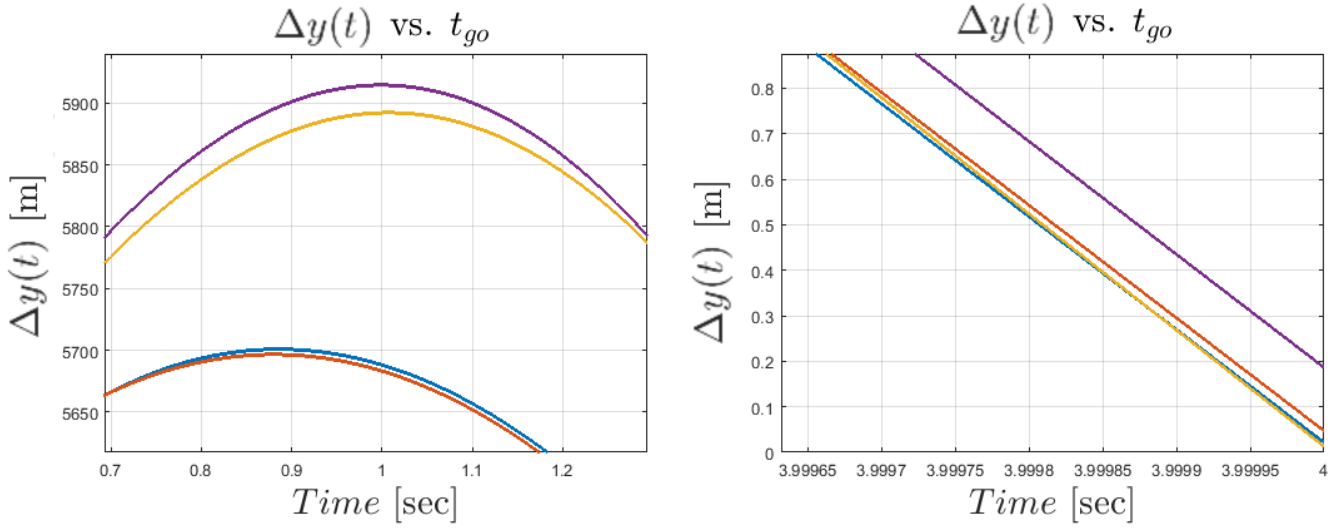

Figure 27: Close up on Trajectories

5 Unbounded u_c Input

In this section we are requested to re-design the auto-pilot gains such that δ saturation will not occur. Let us write the transfer function of $H_{u_c}^{\delta_c}$ of the auto-pilot :

$$H_{u_c}^{\delta_c} = \frac{\phi}{\phi_c} \cdot \frac{\phi_c}{u_c} \cdot \frac{\delta}{\phi} \tag{5.1}$$

$$H_{u_c}^{\delta_c} = (\frac{T}{m})^{-1} \frac{K(s^2 + M_\delta)}{\tau s^3 + (1+K)s^2 + k_{\dot{\theta}} M_\delta s + K M_\delta} \cdot \frac{s^2}{s^2 + M_\delta} \tag{5.2}$$

$$\underline{\underline{H_{u_c}^{\delta_c} = (\frac{T}{m})^{-1} \frac{K s^2}{\tau s^3 + (1+K)s^2 + k_{\dot{\theta}} M_\delta s + K M_\delta}}} \tag{5.3}$$

Under my AP design conditions I simulated the transfer function under a set of u_c's, when the rest of the parameters are just as before. And we shall look look for boundaries :

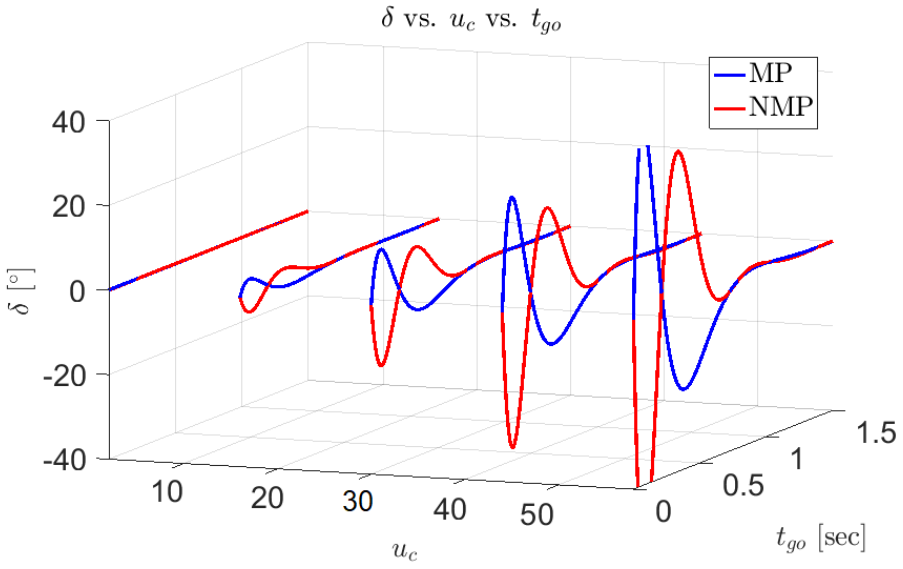

Figure 28: Servo Response to u_c (Original Parameters)

We can see that when changing u_c input via using convolution integral (BIBO), the servo achieves higher results with the same original gains. The maximal boundary for u_c input is around 60 $[\frac{m}{sec^2}]$, whereas MP is slightly more sensitive than the NMP. Beyond that value, we pass the 30 ° limit and losing the desired effect.

5.1 Comparison with Original Gains

After witnessing $\rho_v \Leftrightarrow u_c$ ability to amplify our desired parameter, we'll re-tune the default parameters (**Project 1**) of **K** (state feedback) and $K_{\dot{\theta}}$ (rate feedback) and see the trade-off.

First we'll see what happens when **K** is modified :

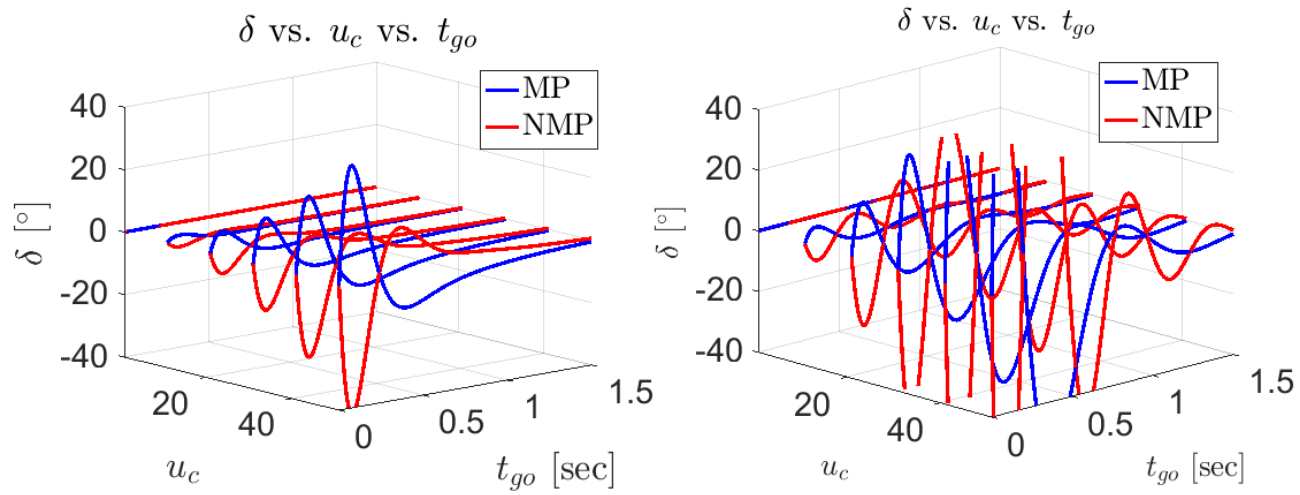

Figure 29: **Left : K** $\downarrow$ δ Stability under u_c **Right : K** $\uparrow$

We can see that **reduction** of K allows us staying at the mechanical boundary of the servo for bigger u_c values. Contrarily, when K is bigger than default value (K > 0.2), u_c diverges quicker and lower the possible operation span.

Now we'll check the influence of $K_{\dot{\theta}}$ modification :

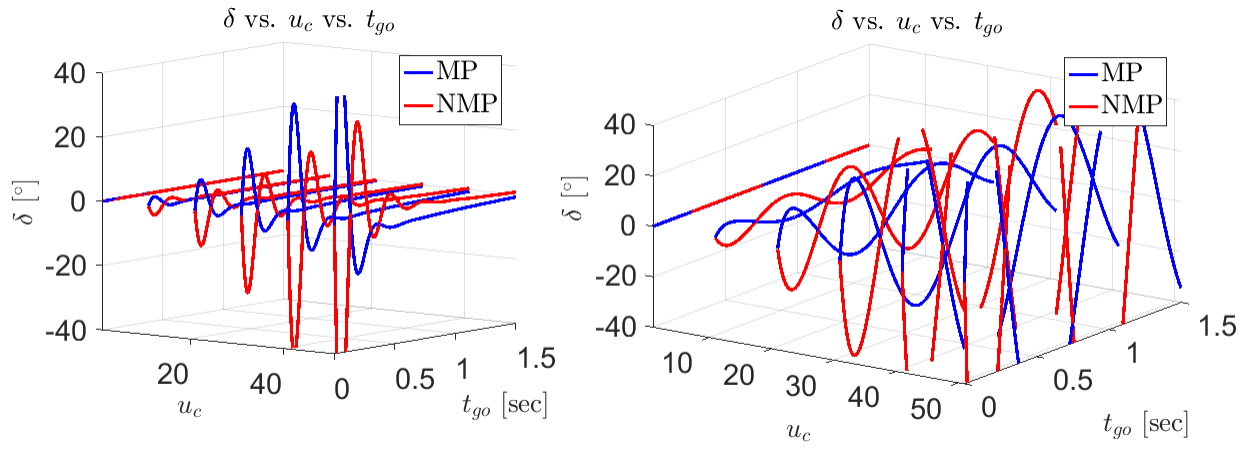

Figure 30: **Left :** $K_{\dot{\theta}} \downarrow$ δ Stability under u_c **Right :** $K_{\dot{\theta}} \uparrow$

We can see somewhat correlation with K modification - u_c amplification is possible in concordance with gain reduction, or nonetheless **retuning**. That phenomenon allows us better performances at lower gain (K, $K_{\dot{\theta}}$) control effort "costs".

5.2 Comparison with section 3.

In this section we are requested to compare N^* results of when ρ_v is at maximal value $\rho_{v,max} \to 60\frac{m}{sec^2}$. Starting with K gain's modification :

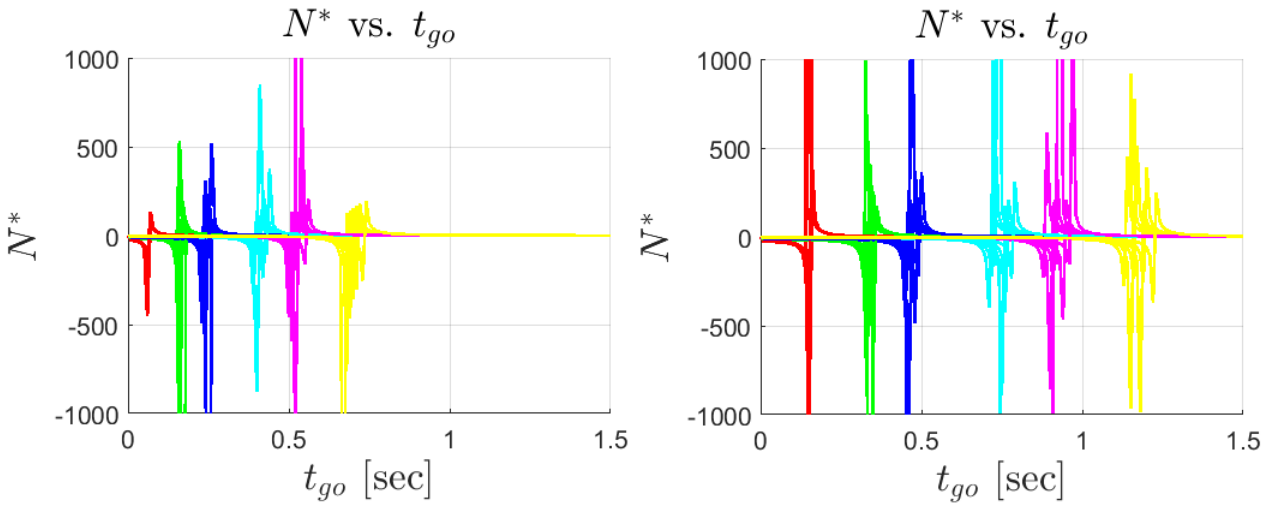

Figure 31: **Left :** **K** $\downarrow$ K Modification **Right :** **K** $\uparrow$

From **Fig.** 31 we can see that when u_c is maximal, the system's sensitivity to K gains increases as well. It is therefore advised to reduce the K gain magnitude. That way, the effective navigation ratio is more moderate.

Now we'll check the influence $K_{\dot{\theta}}$ modification influence on :

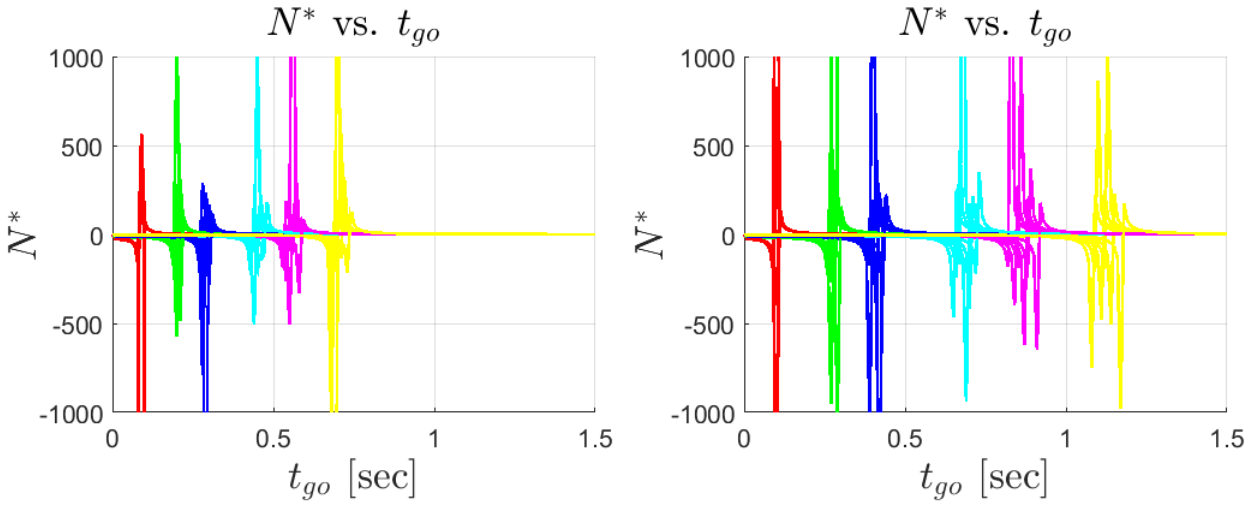

Figure 32: **Left :** $K_{\dot{\theta}} \downarrow$ $K_{\dot{\theta}}$ Modification **Right :** $K_{\dot{\theta}} \uparrow$

Interestingly, $K_{\dot{\theta}}$ has an influence on the N^* peaks timings, perhaps because of his close relation with him being at the same loop with the servo. Either here, the N^* magnitudes show ∞ spikes when $K_{\dot{\theta}}$ increases, and moderate values when $K_{\dot{\theta}}$ decreases.

$-fin-$